FEM simulation of fold-and-thrust belts in the South Central High Andes of Chile and Argentina

FEM simulation of fold-and-thrust belts in the South Central High Andes of Chile and Argentina

Md. Rafiqul Islam and Daigoro Hayashi

Simulation Tectonics Laboratory, Faculty of Science,
University of the Ryukyus, 903-0213, Okinawa, Japan

Abstract

FEM analysis for stress determination of fold-and-thrust belts of the South Central High Andes (SCHA) was carried out on Paleozoic to Quaternary rocks from the Coastal Cordillera to Precordillera regions of the Chile and Argentinean Andes, between 30° and 33° south latitudes. A two-dimensional vertical cross-section including 8 layers through the Andean crust up to Moho has been represented by a finite element model composed of an assembly of 2699 elements and 1456 nodes in a state of plane strain conditions. The model is assumed to be multilayered lithospheric crustal block undergoing convergence, and we choose to demonstrate our results by applying horizontal displacement rate (average velocity of 6.50 cm/yr) of descending Nazca plate. The failure of elements is defined by adopting the concept of Mohr-Coulomb failure criterion. The assigned rock rheology and physical properties of each layer in simulation make the model behavior as elastic body in which well defined failure location gives a hint of thrust development. Studies of lithospheric deformation of the fold-and-thrust belts in this zone where structural style varies from thin-skinned to thick-skinned fold-and-thrust belts have revealed various compressional states of stress. The maximum compressional stress (σ_1) was generally oriented in an E-W direction. Along the westernmost part of the Coastal Cordillera, the strain deformation is extensional in some elements, which can be explained by a co-seismic crustal bending readjustment. Overall study results imply that most of the basement-involved deep thrusts (about 20 km) and deformation, occurred within the upper crustal parts that lie in Layers-4, 5 and 6, are more likely related to crustal anisotropy.

1. Introduction

The Andean Cordillera (Figs 1 and 2) is the world's archetypal example of a subduction-related mountain belt along the western continental margin of South America above the subducting Nazca plate. In this non-collisional geotectonic environment, it is now accepted

Received: January 10, 2007

that the huge amounts of crustal volume related to plateau formation of the Andes (up to 75 km crustal thickness) is principally due to crustal shortening concentrated at the easternmost edge of the Andean orogen during the Neogene (McQuarrie, 2002).

The Andean Cenozoic fold-and-thrust belts from 30°S to 33°S in Chile and Argentina varies in structural style from thin-skinned to thick-skinned and most of which allowed establishment of the age of uplift for the High Andes and shortening along eastern-most edge of the same latitudes (Perez, 2001). Cristallini and Ramos (2000) estimated a total of 136 km shortening in the Precordillera segment, while amount of orogenic shortening was estimated about 18 km in the Principal Cordillera. In this orogenic belt, the thin-skinned structural style is typical of the external zones of fold-and-thrust belts, whereas the thick-skinned style occurs in the hinterland and internal zones (Abascal, 2005). For instances, in the South Central High Andes (SCHA) region (Figs 3 and 4), the classic eastward-verging thin-skinned (about 3-8 km) fold-and-thrust belt develops in Precordillera and westward-verging fold-and-thrust belt develops in Coastal Cordillera, although, in the internal zones including Main and Frontal Cordillera, the dominant structural style is thick-skinned (about 20 km). Jordan et al. (1983) pointed out that this change has been attributed mainly due to inherited crustal properties.

Because of scientific interest, mechanics of fold-and-thrust belts and accretionary wedges have been extensively studied during the last twenty years (e.g., Davis et al., 1983). Some important studies concerning fold-and-thrust belts have focused on the role of rheology of the basal decollement, showing how markedly different wedges develop above a frictional or a ductile layer, respectively (Davis and Engelder, 1985; Costa and Vendeville, 2002; and Koyi and Cotton, 2004). Some other studies on thrust systems have paid particular attention to the style of thrusting, changes in fault attitude, displacement rate and amount of ramp angle. In general, the structural evolution of a thrust system depends on stratigraphy, mechanical property of the rocks, duration and rate of deformation and uplift versus subsidence ratios (Doglioni and Prosser, 1997). In particular, the mechanical property, rheological characteristics of the layers of the deformed rocks (e.g. presence of competence contrasts) appeared to be of great significance in influencing the final geometry of the structures and the kinematics of the thrust system (Koyi et al., 2004).

Fold-and-thrust belts along 30-33°S of the South Central High Andean area are characterized by deformed belt of Mesozoic and Cenozoic sedimentary and volcanic rocks that overlie the Permo-Triassic volcanic basement of the Choiyoi Group (Ramos et al. 1996). Most of the deformations occurred within Choiyoi group. The deformation style of the Choiyoi basement and the sedimentary cover are very different. Their contrasting rheological properties are one of the factors that contribute to the complex structure of the region (Cristallini and Ramos, 2000). Although, rheological characteristics of strata in different fold-and-thrust belts allover the world has been studied extensively in different

mountain belts (e.g. McQuarrie, 2004) during the last twenty years, but, in this part of the Andes, it is still obscure. In this circumstances, an important factor like numerical modeling have been taken into account to show experimentally the rheological effects on the tectonic deformation in the upper crust of the South American plate by applying displacement/absolute velocity rate of descending Nazca plate along the flat-slab subduction zone. In this study, significance of rheology on fold-and-thrust belt systems has paid particular attention. We concentrate to get rheological insights into the development of basement-involved thrust belt by applying elastic finite-element modeling techniques. Thus, this contribution is an extensive attempt after Cristallini and Ramos, (2000) and to provide new insights into the mechanics of basement-involved deformation of the Andean belts present at this latitude. Three major objectives of this study are:

(1) to ascertain the nature of stress that could be interpreted as a potential rupture zone and provide an estimate of the possibility of failure as faults developed along core of the South Central High Andes,

(2) to establish the geometry and mechanical behavior especially rheological link between basement-cover and basement-involved E-W vergent thrusting of the area, and

(3) to correlate thin-skinned and thick-skinned deformation in this region to events in entire Andean orogeny and consider the main factors controlling deformation.

1.1. Materials and Methods

(1) Geological cross-section prepared by Cristallini and Ramos (2000)
(2) Physical properties of strata of the cross-sectional area
(3) Finite Element Mesh
(4) Finite Element Program by Hayashi (unpublished)
(5) Mohr-Coulomb Failure Criterion
(6) Focal-Mechanism Solutions of study area

Three-steps of study have been considered by using aforesaid materials

(i) At the first step, the belt geometry *i. e.* a geological cross-section (Fig.4) presented by Cristallini and Ramos (2000) after Introcaso et al. (1992) is highly simplified (Fig.5). Then the study is focused on the identification of the main geometric and rheological parameters controlling the deformation in fold-and-thrust belts of this region by a numerical model.

(ii) In the second step, concentration was made to calculate principal stresses that could be interpreted as a potential repture zones and give an estimate of the possibility of failure of elements from the concept of Mohr-Coulomb Failure Criterion.

(iii) In the third step, the rheological role of basement-involved uplift is introduced within the belt and its effect on the deformation pattern is examined by Focal-Mechanism Solutions.

1.2. Limitations

The present study, elastic mechanical analysis of SCHA fold-and-thrust belt contained in brittle crust, was performed using finite element code by Hayashi (2002). The program has been applied to two-dimensional geometry. The modeling approach restricts the interpretation to the most robust features of the experiments. The Mohr-Coulomb rheology is obviously inappropriate to represent the weak rocks of both the upper and lower layers, and we considered only approximate upper layers weakening by principal shear-stress at the model layers. Hence we are confident that the comparison of the general tectonic features, e.g. the distribution and propagation of thrusts, style of thrusting, changes in fault attitude, displacement rate and amount and ramp angle are little affected by the limitations of the modeling technique. Although the correlation to natural orogens remains qualitative, but allows intuitive understanding of the tectonic evolution of fold-and-thrust belts in this region. In any case, we have to bear in mind that interpretations of the modeling results remain quantitative because of the intrinsic limitations of numerical modeling.

2. Tectonic setting of the South American Plate (SAP)

The tectonics of the South American plate (SAP) (Fig.1), which is not attached to any significant length of subducting slab, is dominated by non-slab tectonic forces such as those due to lateral density variations within the lithosphere (i.e., cooling oceanic lithosphere, associated with "ridge push", acting outward from the Mid-Atlantic Ridge; the Brazilian continental margin; and elevated topography of the Andes) and forces transmitted across collisional boundaries along the Peru-Chile Trench. The SAP therefore provides an ideal location to investigate the relative contributions of non-slab tectonic sources within the lithosphere. The South American plate consists of about equal amounts of oceanic (51%) and continental (49%) lithosphere. The young oceanic lithosphere (younger than 66 Ma) makes up of about 35% of the plate area, and old oceanic lithosphere makes up about 16%. The continental areas are divided between submarine passive margins (10%) and regions above sea levels (about 39%). The mean elevations of the whole plate and of oceanic and continental areas are about -2100, -3800, and +600m respectively (Coblentz and Richardson, 1996). The boundary geometry of the South American plate (Fig.1) is as follows as mentioned by the aforesaid authors:

(i) The plate is attached to only about 500km of subducted slab, mostly along the Lesser Antilles and South Sandwich Trenches.

(ii) In contrast, convergent boundaries make up more than 9000km of the plate boundary, the majority of which is associated with the subduction of the Nazca plate beneath the western margin of the South America. Subduction occurs along the entire western boundary of the plate.

(iii) North of 45°S, the Nazca plate subducts under South America, and the axis of the Peru-Chile Trench (PCT) define the western margin of the South America plate.

(iv) South of 45°S, the Antarctic plate subducts under South America along the Antarctic-Chile Trench (ACT). Most of the southern boundary is defined by the Scotia margin (SCO).

(v) The eastern plate boundary, defined by the Mid-Atlantic Ridge (MAR), is characterized by high topography of ocean floor. This ridge system extends more than 7000 km, making it nearly equal in length to the convergent boundaries.

(vi) The boundary between North and South America (NAM) is diffuse and in therefore poorly constrained.

2.1. Segmentation of the subducted Nazca Plate

The Andes mountain system is commonly used as an illustration of a "simple" orogen formed by subduction of an oceanic plate beneath a continental margin. Over much of its length, the Andes consist of a magmatic arc, flanked on the west by a trench and on the east by a foreland thrust belt and basin. These characteristics of an "Andean-type margin" are recognized in the geological record of various convergent margins. Although the Andes are morphologically continuous along strike for more than 4000 km (from about 5 °S to 45°S), distinct broad-scale tectonic segments can be identified (Fig. 2). These tectonic segments are located above segments of similar scale in the subducted Nazca plate, defined by major along-strike variations in the deep of the Benioff zone. The coincidence of lateral variations in the geometry of the descending Nazca plate and in the Andean physiography and geology is remarkable (Jordan et al., 1983).

South of Ecuador, the descending Nazca plate is divided into four major segments as inferred from the spatial distribution of intermediate-depth earthquakes. From about 2°S to 15°S and 27° to 33°S, the Benioff zone dips only about 5° to 10° east, whereas from 15°S to 24°S and south of 33°S, the zone inclined about 30° east (Fg.2). At the north end of the Chile-Argentina flat-subducted slab (Fig. 3), there is gap along strike (between 24°S to 27°S) in the distribution of the intermediate-depth (125-300 km) earthquakes. The mean mantle in this area appears to be virtually aseismic. Continuity of fore-arc features and magamtic-arc features suggests that the major change from steep to flat subduction occurs near 27°S. Above the aseismic region, there is an area of complex transitional tectonics in the upper plate. The down-dip lengths of the two nearly flat segments of the subducted plate are similar, about 750 km measured from the axis of the trench to a depth of about 160 km. The intervening more steeply dipping segment is slightly shorter, about 650 to 700 km to depth of about 300 km. The segment south of 33°S is significantly shorter, less than 500 km measured down-dip from the trench axis to 160 km depth (Jordan et al., 1983).

Generally, subduction at angles of 25-30° is called "subduction of normal type",

meaning a subduction of the Chilean type. On the other hand, "subhorizontal or flat-slab subduction" makes reference to a gentle dip angle of 15° or less. Subhorizontal or flat-slab subduction occurs in central Chile and it is correlated to characteristics phenomena at the surface. First, no Quaternary volcanic activity is present over this gentle angle subduction zone, thus defining an important gap in the actual Andean volcanic arc. Second, there is

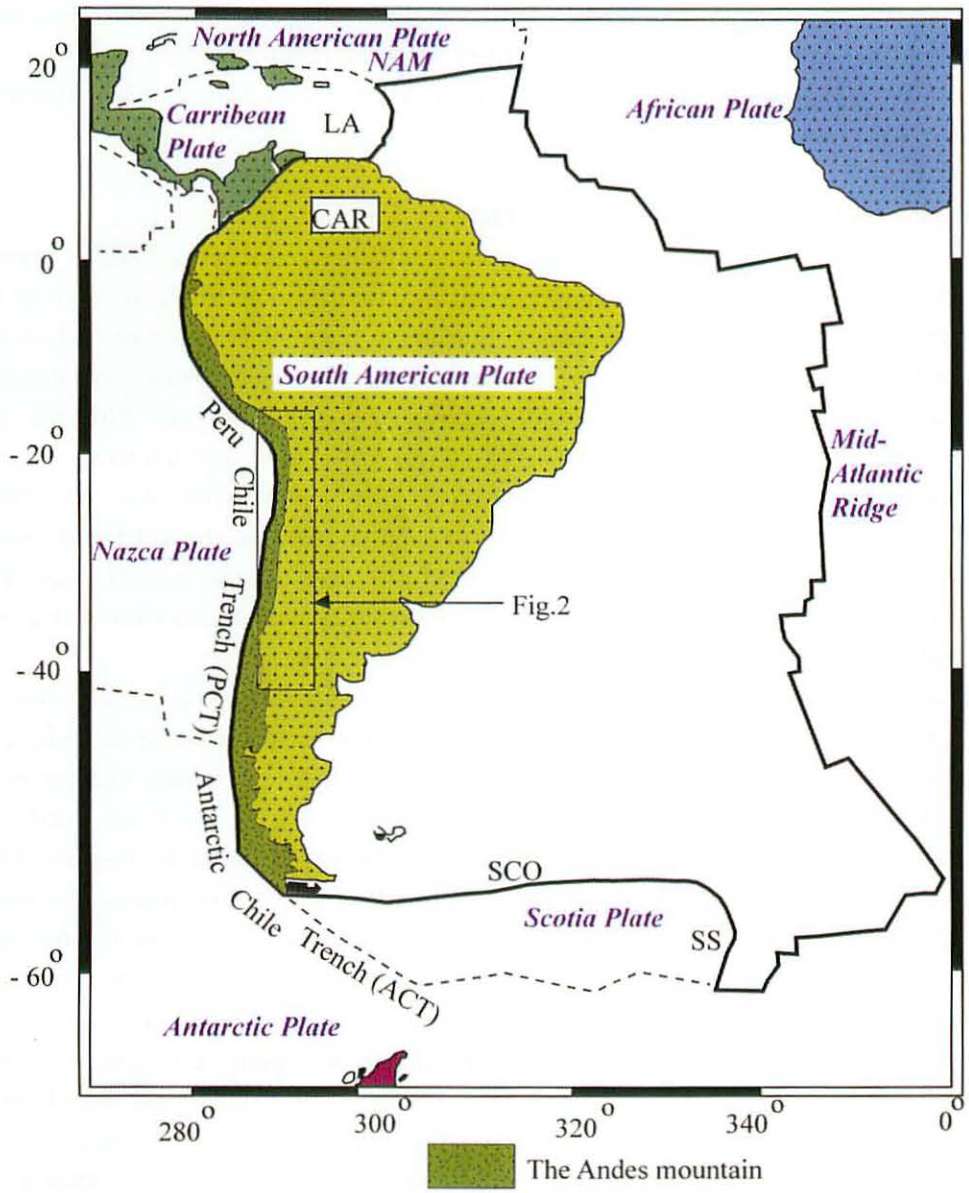

Fig.1 South American Plate with boundaries (after Coblentz and Richardson, 1996). Abbreviations are SCO, Scotia margin; SS, South Sandwich Trench; LA, Lasser Antilles arc; and CAR, Caribean

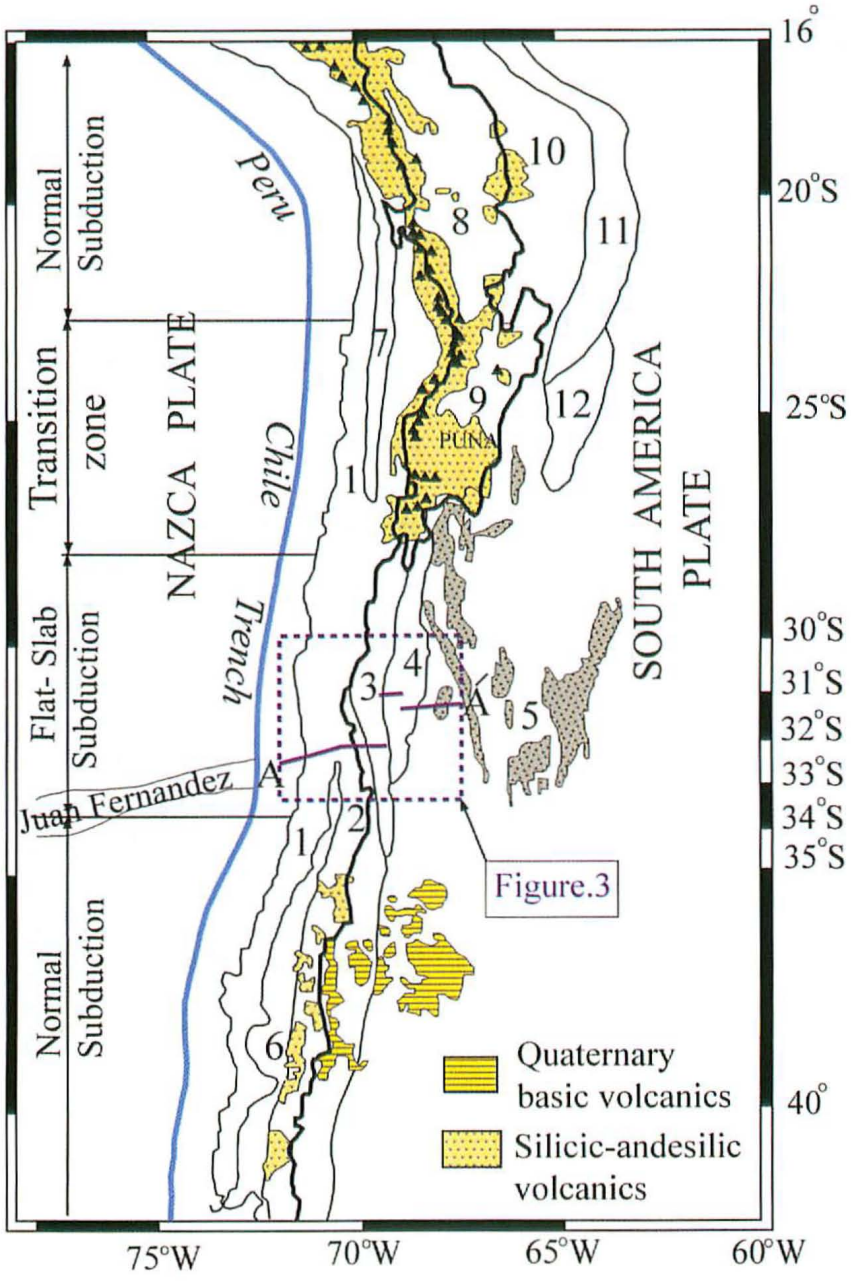

Fig.2 Tectonic provinces and young volcanics cover of the central Andes in Chile, Bolivia and Argentina. Heavy line marcks Andean crest (from Jordan et al.,1983). Solid Triangles are active volcanoes of the Central and Southern Volcanic Zones (Chaill and Isacks, 1992). The Central Andes are subdivided into Altiplano,Puna and Flat-Slab segments (from Jordan et al., 1983; Kley et al., 1999). 1 = Coastal Cordillera, 2 = Principal or Main Cordillera, 3 = Frontal Cordillera, 4 = Precordillera, 5 = Sierras Pampeanas, 6 = Central Valley, 7 = Longitudinal Valley, 8 = Altiplano, 9 = Puna, 10 = Eastern Cordillera, 11 = Subandean belt, 12 = Santa Barbara

an absence of a central valley in central Chile. (Cahill and Isacks, 1992).

Beneath the central Chile and western Argentina (28-33°), the subducted Nazca Plate has a low dip angle (<10°) being almost subhorizontal, and it extends eastward for hundreds of kilometers at a depth of about 100km before reassuming its downward descent (e.g. Cahill and Isacks, 1992). The different structural provinces of the Central Andes were controlled by the Wadati-Benioff subduction geometry. A flat subduction segment without arc magmatism that underlies the Precordillera and Sierras Pampeanas structural provinces, is recognized north of 33°30' with subduction angles between 5 and 10°. The segment to the south of this latitude has arc magmatism and an average dip of the oceanic slab beneath the continent of 30°. The flat slab configuration between 28-33°S resulted in a strong contractional tectonics for more than 1000km inland into the Sierras Pampeanas, where thick-skinned tectonics is observed (Jordan et al., 1983).

2.2. Segmentation of upper-plate geology in Argentina-Chile-Bolivia

The regional geologic framework of the Andes in southern Peru, Bolivia, Chile and Argentina has been extensively described different authors. The Andean convergent margin is a region of intense crustal deformation, with six great subduction earthquakes (M 7.8) in this century. The regional pattern of seismicity and volcanism shows a high degree of segmentation along strike of the Andes. Segments of steep-slab subduction alternate with aseismic regions and segments of flat slab-subduction. This segmentation is related to heterogeneity on the subducting Nazca Plate (Gutscher et al., 1999).

Areas above the 30°-dipping Benioff zone, the outer trench slope has normal faults, a major valley divides coastal mountains from the Andean range with its active volcanoes, and the foreland is primarily deformed by thin-skinned shortening. In contrast, areas over a flat-subducting Nazca plate include less faulting in the outer trench slope, no longitudinal valley, no active volcanoes, and foreland deformation is dominated by a combination of thin-skinned thrusting and shortening of the basement. In the eastern Andes and foreland regions, based on cross-section, four distinct segments were recognized by Jordan et al., (1983). That are-

(1) the Bolivian Altiplano, the eastern Cordillera, and the Subandean zone, between 15°S and 23°S,

(2) a "transition zone" comprising the Argentine Puna, Eastern Cordillera, and Santa Barbara system between 23°S and 27°S,

(3) the Frontal Cordillera, the Precordillera, and Pampeanas Ranges between 27°S and 33°S, and

(4) the eastern parts of the Cordillera Principal and areas of widespread basaltic volcanism south of 33°S (to 46°S).

Segment 3 coincides with the nearly flat segment of the subducted Nazca plate, whereas segments 1, 4 and probably 2 coincide with 30°-dipping segments of the subducted plate.

Our study area, SCHA, is located within the segment 3 (see Fig.3).

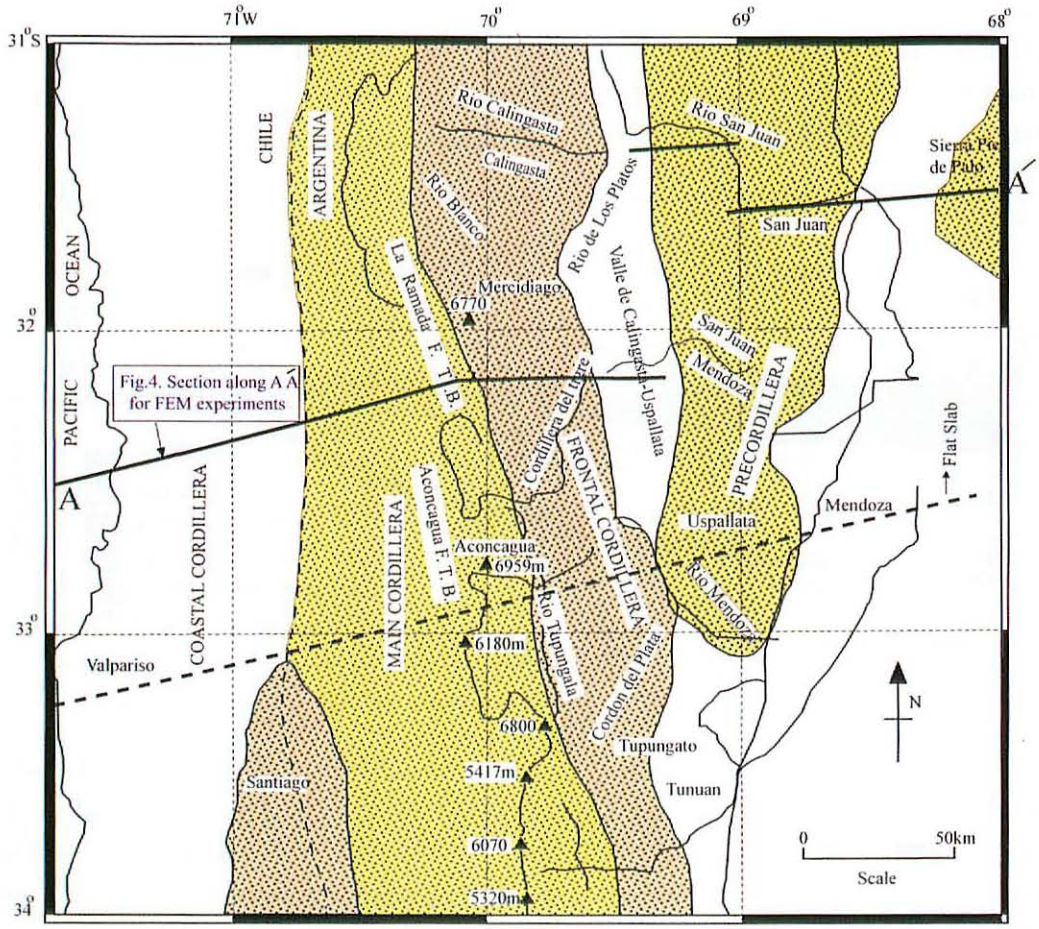

Fig.3 Geological setting of the flat-slab region in the Central High Andes, Argentina and Chile. The solid lines indicate the cross-section along 32°SL. Dashed line indicates the approximately boundary between the flat-slab (10°) and 30° dipping subduction zone, F.T.B = Fold and Thrust Belt (Cristallini and Ramos, 2000)

3. Geology of major geo-tectonic units in the SCHA, Argentina-Chile

The Andean Cordillera is the classic example of a mountain chain formed during the subduction of an oceanic slab under a continental plate. In this non-collisional geotectonic environment, it is now accepted that the huge amounts of crustal volume related to plateau formation of the Andes (up to 75 km crustal thickness, Yuan et al., 2002) is principally due to crustal shortening concentrated at the eastern-most edge of the orogen during the Neogene (Kley et al., 1999 and McQuarrie, 2002). But a remaining question is how to relate this building mechanism at a lithospheric scale with the processes occurring at the western side of the orogen where the Nazca and South American plates are actually

interacting. There are still no appropriate answers to this question (Tassara, 2005). In the SCHA, along latitudes between 30-33°S, five giant geo-tectonic units existed from west to east, such as - (1) Coastal Cordillera in the western region, (2) Principal or Main Cordillera in the central region, (3) Frontal Cordillera in the central region, (4) Precordillera and (5) Sierras Pie de Palo (Sierras Pampaenas Ranges) in the eastward foreland region (Fig.4).

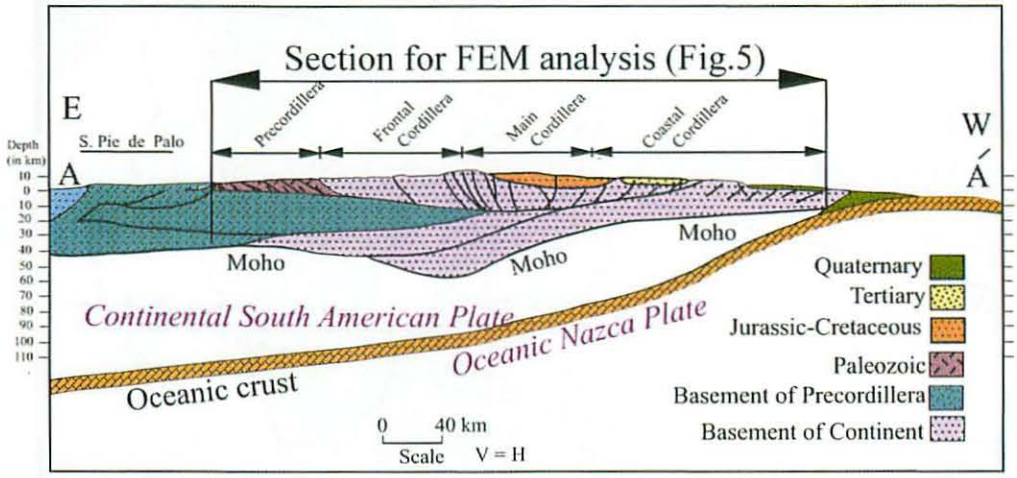

Fig.4 Andean section along 32°SL (location in Fig.3) (Cristallini and Ramos, 2000)

Based on the degree of basement involvement, Ramos et al. (1996) divided the fold-and-thrust belts of the Principal and Frontal Cordillera into three distinct segments as (1) La Ramada, (2) Aconcagua (see Fig.3), and (3) Malargiie fold and thrust belts. The prime structural differences among these three distinct segments regarding tectonic evolution in the South Central Andes are-

(i) In the north, the La Ramada fold and thrust belt is combined thin-skinned and thick-skinned with basement-involved and is the result of tectonic inversion of a Late Triassic rift system,

(ii) The central Aconcagua fold and thrust belt is a thin-skinned system with no basement involved, and

(iii) While to the south, the Malargiie belt is also the result of tectonic inversion of a Late Triassic-Early Jurassic rift system.

As a consequence, the Principal and Frontal Cordilleras in the La Ramada and Malargiie segments are similar. Blocks of the Permo-Triassic basement are included in both Cordilleras. In contrast, in the Aconcagua segment the Frontal Cordillera is a single, huge block of this Permo-Triassic basement, which is not exposed in the Principal Cordillera (Ramos et al. 1996). Geology of the five major geo-tectonic units including La Ramada segment is described successively as follows.

3.1. Coastal Cordillera

The 3-13 km thick sequence of volcanic rocks that extends 1200 km along the Coastal Range in central and north central Chile is mainly represented by highly porphyritic (20-30% phenocrysts) lavas with unzoned Ca-rich plagioclase (Morata and Aguirre, 2003). Between 33°40 and 34°5 S, the Coastal Cordillera is largely composed of extensive Mesozoic granitoid batholiths, as well as Paleozoic metamorphic and plutonic rocks. The contact between the basement and the Jurassic-early Cretaceous plutonic complexes has been described as a ramp-flat extensional fault system. This extensional fault system has been related to a retreating subduction boundary (Taylor et al., 1998). Important extension is recorded in Triassic times along the Coastal Cordillera and in the Principal Cordillera after the amalgamation of Pangea (Alvarez and Ramos, 1999).

3.2. Principal or Main Cordillera

Cenozoic shortening in the Main Cordillera started at the time 22-20 Ma both in the northern and southern portions of the Andean region between 30-34°S (Ramos, 1996). At this time, the volcanic front was active along the Chilean slope of the Principal Cordillera. The Farellones volcanic arc was active, and thick sequences of andesite, dacite, and rhyolite lavas and pyroclastic rocks were unconformably covers over large areas (Ramos et al. 2002). The absence of Quaternary volcanism in the present-day flat slab region results from the absence of asthenospheric wedge underneath the continent (Jordan et al., 1983). According to Ramos et al., (2002) the main deformation phases and uplift of the thin-and thick-skinned fold and thrust belts of Principal Cordillera occurred between 20 and 8.6 Ma.

3.3. Frontal Cordillera

In the South Central High Andean region, between 30° and 33°S, La Ramada fold-and thrust belt is one of the prime tectonic structures in the Frontal Cordillera (Fig. 4) and is dominantly a product of the Cenozoic Andean orogeny. The La Ramada segment is located to north of Aconcagua, and consists of a series of basement uplifts such as the Santa Cruz, Mercedario-Ramada, El Espinacito and La Cerrada Cordilleras.

This fold-and-thrust belt at 32°S, allowed establishment of the age of uplift and shortening for the High Andes at these latitudes (Perez, 2001), and is characterized by a deformed belt of Mesozoic and Cenozoic sedimentary and volcanic rocks that overlie the Permo-Triassic volcanic basement of the Choiyoi Group (Ramos et al., 1996). The deformation style of the Choiyoi basement and the sedimentary cover are very different. Their contrasting rheological properties are one of the factors that contributes to the complex structure of the region (Cristallini and Ramos, 2000).

Folding and thrusting are the main mechanisms by which geologic structures are internally thickened and shortened. In many cases, the basal detachment horizon is located

above a rigid crystalline basement near the base of the sedimentary sequences. This style of deformation, in which the basement remains undeformed is referred to as "thin-skinned tectonics"(Epard and Escher, 1996). The Cenozoic structural evolution of the fold-and-thrust belt in the High Andes of Chile and Argentina, around 32°S, shows in time and space the interaction of thin-skinned and thick-skinned deformations (Cristallini and Ramos, 2000). In case of "thick-skinned tectonics" the basement is deformed prominently as found in the deep structures of the South Central High Andean areas. The major thrusts have relatively steep dips (>55°), even those faults close to the foreland. The structural style is depicted in the cross-section (Fig.4) where two levels of detachment can be inferred. The lower one is controlled by basement, which underlie about 20 km, and the upper (about 3-8km) one that lies in the gypsum-rich sequence of the Auquilco Formation (Late Jurassic). The lower detachment level was based on geometric constrains. Most of the main ranges at the Ramada fold and thrust belt are controlled by the lower detachment (Ramos et al., 1996).

In deep structures of the La Ramada fold-and thrust belt three deformational stages have been identified by Cristallini and Ramos (2000), these are:

(i) The first started with N-NNW-trending structures (Cordillera de Los Penitentes, Cordillera del Medio) detached in upper Jurassic gypsum, and is typical of a thin-skinned fold and thrust belt.

(ii) In the second stage, the basement is involved by tectonic inversion of Triassic normal faults producing a thick-skinned fold and thrust belt that refolded older structures (Cordillera Casa de Piedra), and consequently a passive and ductile deformation of post Jurassic deposits took place.

(iii) The basement deformation with high-angle reverse faults at the Ramada-Espinacito massif terminated at the east border of the Triassic rift system producing a sticking point in that sector. This was responsible for the third stage, characterized by NNW out-of-sequence thrusts developed in the westernmost sector.

3.4. Precordillera

The present-day tectonics and uplift of the South Central High are concentrated further west in Sierra de Pie de Palo i. e. in Precordillera. The 50 km wide Precordillera thrust belt is situated in the western part of the Sierra de Pie de Palo (Ramos et al., 2002). East of the Precordillera is the Bermejo Basin, a foreland basin located between the thin-skinned thrust belt and thick-skinned basement uplifts of the Sierras Pampeanas further east (Jordan et al., 1993). The Precordillera itself has classically been divided into Eastern, Central and Western belts based on Andean and pre-Andean geological characteristics. The eastern Precordillera consists of mostly west-verging structures that probably involve basement. The Central and Western Precordillera form an east-verging package of mostly emergent thrusts faults that carry Paleozoic and younger cover rocks. At the La Ramada

latitudes, the main shortening was assimilated in the Precordillera fold and thrust belt. A total of 136 km shortening was estimated in the Precordillera segment. A total of 122 km contraction was obtained for the Western and Central Precordillera and 14 km in the Eastern Precordillera. It is interesting to note that the maximum surface shortening was found in the Precordillera sector, while the maximum crustal shortening was located under Frontal Cordillera (Cristallini and Ramos, 2000). At least three major brittle deformational periods have been recognized in the Precordillera. The majority of the brittle deformational occurred during the late Tertiary Andean orogeny (Ramos et al., 1996).

3.5. Sierras de Pie de Palo (Sierras Pampaenas)

The Pampean flat-slab segment of the greater Andean orogenic system can be defined in part by a gap of active arc volcanism in the main Andes. Present-day tectonics and uplift are concentrated further west in Sierra de Pie de Palo (Fig. 4). This neotectonic activity matches the Eastern Precordillera uplift during late Quaternary times. Geologic evidence in the Sierra de Pie de Palo indicates that the range was covered by late Pliocene distal synorogenic deposits derived from the Precordillera (Ramos et al., 2002). Uplift of the basement blocks of the Sierras Pampeanas was the result of Andean compression during late Cenozoic times. Tilting and rotation of the mountain blocks were controlled by décollments at the depth of the brittle-ductile transitions in the basement located at different depths. On the basis of the location of intraplate focal mechanisms two décollement levels were proposed, one at about 12-15km and another at 22-25km depth as illustrated by Jordan et. al (1983 and 1993).

4. Numerical modeling in the Andean region

To our knowledge, the first numerical analysis for the evolution of deformation and topography of high plateau of the Andes was carried out by Wdowinski and Bock (1994). A temperature dependent viscoplastic flow model of continental lithosphere was used to investigate the evolution of deformation and topography of the high-elevated plateaus like Altiplano and Puna. Richardson and Coblentz (1994) performed an elastic finite element analysis of the lithospheric stress field in the Cordillera Blanca region of Peru to evaluate the lithospheric stress state and constrain the South American intraplate stress magnitudes. A two-dimensional finite element grid consisting of an assembly of isotropic, elastic quadrilateral elements in a state of plain strain was used to represent the lithosphere. Their modeling results indicated bounds of 10 MPa and 75 MPa for the magnitude of the average horizontal stress averaged over the 100km thick lithosphere. Coblentz and Richardson (1996) represented another finite element analysis concerning intraplate stress field of the South America to evaluate the relative contribution plate

boundary forces and intraplate stress sources. Hereafter, Talukder and Hayashi (2006) applied a two-dimensional finite element modeling technique to analyze the state of stress and the fault development within the Subandean foreland region of Southern Bolivia and Northern Argentinean Central Andes assuming the lithospheric crustal block as a multilayered elastic slab exhuming under plain-strain condition. In this study, we take an approach similar to that of Richardson and Coblentz (1994); Talukder and Hayashi (2006) and use an elastic rheology dependent model to investigate large-scale compressional lithospheric deformation regarding thin-skinned and thick-skinned fold-and-thrust belts in the South Central High Andes.

5. The Model

5.1. Location and configuration

The modeling performed in the present study was conducted along the profile shown in Fig.4. The profile is centered on 31°40 to 32° 50 S. This vertical cross-section is based on

Table 1a Proposed layers, equivalent stratigraphic units, Formation/ Group and common rock constituents

Layers	Stratigraphic units	Fomations/ Group	Prime rock types	References
Layer-8	Quaternary sediments	Farellones Formation	Breccias and volcanic agglomerates, with white acid tuffs, andesitic lavas	Cristallini and Ramos, 2000
Layer-7	Tertiary strata	Farellones Formation	Breccias and volcanic agglomerates, with white acid tuffs, andesitic lavas	Cristallini and Ramos, 2000
Layer-6	Cretaceous	Diamante and Juncal Formation, Mendoza Group	Red sandstone, conglomerates, breccias and volcanic aglomerates	Cristallini and Ramos, 2000
	Jurassic	Tordillo, Auquilco, La Manga, Los Patilos Formation	Red sandstone, gypsum, yellow and gray-green mudstone, green shales	Cristallini and Ramos, 2000
Layer-5	Trissaic	Choiyoi Group	Rhyolitic ignimbrites, granite intrusions	Cristallini and Ramos, 2000
	Upper Paleozoic	Upper Paleozoic Formation	Marine sediments intruded by Permian granites	Cristallini and Ramos, 2000
Layer-4	Lower Paleozoic	Cerro Morado Formation	Sandstone, conglomerates, mudstones associated with minor gypsum	Jordan et al., 1983
Layer-3	Basement	Paleozoic Basement	High-grade metamorphic rocks and granitoid intrusions.	Lucassen et al., 2002
Layer-2	Basement	Paleozoic Basement	High-grade metamorphic rocks and granitoid intrusions.	Lucassen et al., 2002
Layer-1	Basement	Paleozoic Basement	High-grade metamorphic rocks and granitoid intrusions.	Lucassen et al., 2002

a density structure and is consisted with the available crustal information for the Andean region based on seismic and gravity data (Introcaso et al., 1992; Crislallini and Ramos., 2000). The lower crustal lithospheric boundary remains up to Moho discontinuity that lie at depths 10-30 km under Coastal Cordillera, 35-60 km under Principal Cordillera, 60-69 km beneath the Frontal Cordillera and 40-50 km under Precordillera which makes like a concave curve beneath the crust at different depths. The crustal lithosphere was simplified (Fig.5) and was divided into eight layers as Layer-1 to 8 (see Table 1) based on density variations and individual rock layers from Paleozoic basement to Quaternary sequence. The model is extended up to 410.50 km and consists of a 69 km thick continental lithosphere that thins towards trench as it overrides the subducting oceanic lithosphere. This two-dimensional vertical cross-section through the Andean crust up to Moho has been represented by a finite element model (Fig.6) composed of an assembly of 2699 elements and 1456 nodes in a state of plane strain conditions. Lithospheric deformation along aforesaid latitudes is dominated by compressional regime. Compression is well documented, with many examples of thin-skinned and thick-skinned fold-and-thrust belts including Precordillera, in Frontal Cordillera and Principal Cordillera. The major fold-and-thrust belt zone in the modeled area is over 400 km and shows E-W compressional characteristics.

Wdowinski and Bock (1994) stated that the lithospheric deformation in this region is driven by tectonic (surface) and buoyancy (body) forces. Tectonic forces are induced by a subducting plate that shears the overriding plate along the slip layers and horizontally indents the overriding plate inland. Buoyancy forces arise in response to horizontal

Table 1b Layers, covering geotectonic units, prominent geologic structures and generalized sketch of fold-and-thrust belts

Layers	Covering geotectonic units	Prominent geologic structures	Generalized Sketch of fold-and-thrust belts
Layer-1	Coastal Cordillera, Main Cordillera, Frontal Cordillera, Precordillera, Sierras Pampeanas.	Some extensional faults beneath Coastal Cordillera	Layers 4, 5 and 6
Layer-2	Main Cordillera, Frontal Cordillera, Precordillera	No geologic structure	
Layer-3	Frontal Cordillera, Precordillera	No geologic structure	
Layer-4	Precordillera	Numerous blind thrusts up to about 4-8 km in depths	
Layer-5	Main Cordillera, Frontal Cordillera and partially Coastal Cordillera.	Enormous gigantic thrusts ranges from surface to 20 km in depths	
Layer-6	Main Cordillera	Some thrusts are visible	
Layer-7	Coastal Cordillera	No thrust	
Layer-8	Coastal Cordillera	No thrust	

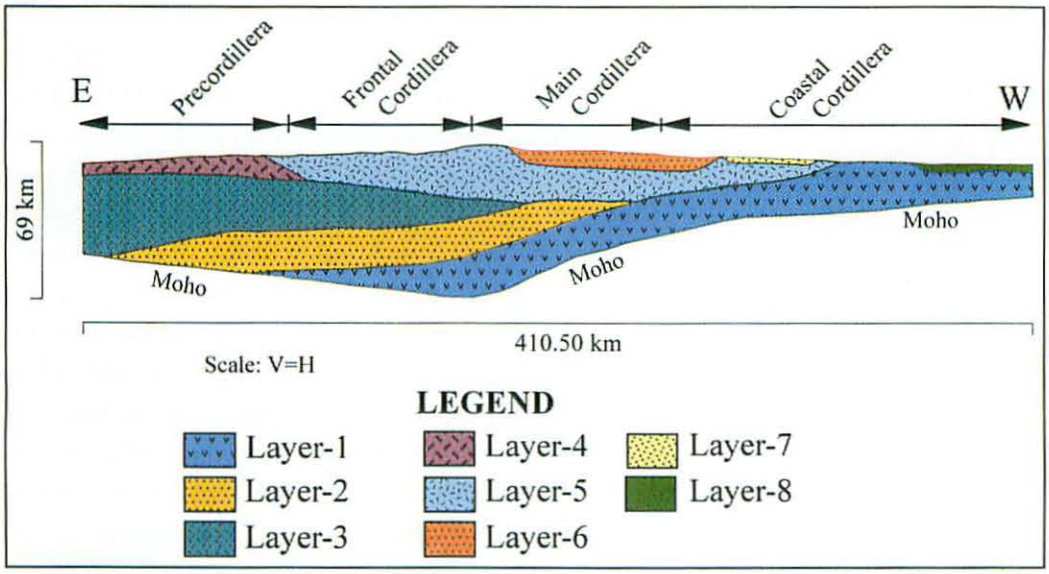

Fig.5 Simplified geological cross-section (modified after Cristallini and Ramos, 2000))

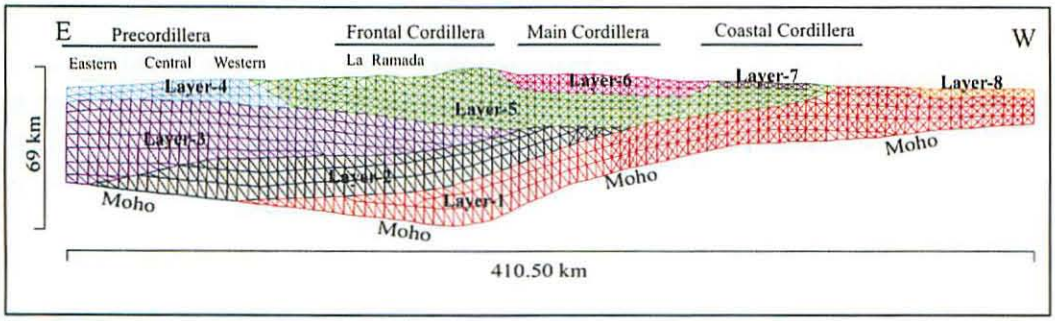

Fig.6 Finite element mesh and model configuration. The model is composed of 2699 triangular elements and 1456 nodes

density gradients, which change with time as the topography and crustal structure evolve. As the deformation evolves, the overriding plate shortening occurred as a result of the horizontal indentation by the underthrusting plate. Cristallini and Ramos (2000) assumed that crustal material is preserved resulting in crustal thickening in response to the horizontal shortening in this region.

5.2. Choice of rheology and physical properties of the model

Wdowinski and Bock (1994) stated that deformation in the central Andes occurred by brittle failure at low temperatures, when the maximum shear stress difference between the largest and smallest principal stress axis [$S = S_1 - S_2$] reaches the yield stress.

In our model, the crust up to 69 km is assumed to behave as an elastic material over

Table 2 Physical parameters applied in the finite element modeling

Layers	Density (ρ)	Vp (km/s)	Vp/ Vs ratio	Vs (km/s)	Poisson's Ratio (υ)	Young's Modulus (E) GPa	Cohesion (C) MPa	Friction angle (ϕ)
L - 1	2960.0	7.00	1.74	4.02	0.253	127.80	185	80
L - 2	2960.0	7.20	1.74	4.14	0.253	124.30	165	75
L - 3	2960.0	6.90	1.74	3.96	0.253	120.80	160	65
L - 4	2800.0	5.20	1.74	2.99	0.253	90.30	145	45
L - 5	2800.0	6.70	1.74	3.85	0.253	107.60	115	35
L - 6	2800.0	5.30	1.74	3.05	0.253	65.50	110	45
L - 7	2670.0	5.20	1.74	2.99	0.253	60.50	100	50
L - 8	2670.0	5.00	1.74	2.87	0.253	57.80	100	45
	Introcaso et al, 1992	Introcaso et al, 1992	Graeber and Asch, 1999	Calculated	Calculatedby equation (1)	Calculated by equation (2)	Sydney et al., 1966	Sydney et al., 1966

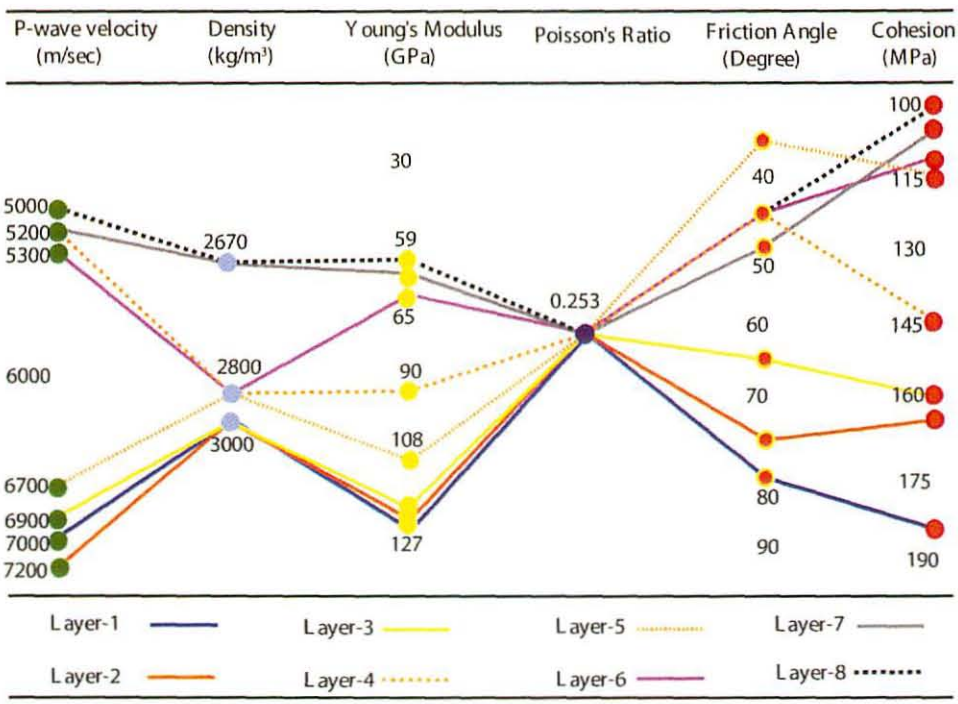

Fig.7 Graphical illustration of physical parameters of different litho-units (Layers) in the South Central High Andean region

geologic timescale. In order to incorporate the brittle deformation mechanisms of the model, we adopt an elastic rheology as imposed by Richardson and Coblentz (1994). In their elastic finite element analysis to evaluate the lithospheric state of stress, they calculated lower and upper bounds of 10 MPa and 75 MPa for the magnitude of the

average horizontal stress averaged over a 100-km thick lithosphere. So, the results of rheological profiles of the aforesaid authors make it possible to assume with reasonable confidence an elastic behavior for the materials in this region as far down as 69 km.

Five prime mechanical properties for individual rock layers such as density, Young's Modulus, Poisson's ratio, friction angle and cohesion used in experiment are listed in Table 2 and Fig.7. The density values were obtained from a 2D Andean crustal gravity-seismic model along 33°S that was carried out by Introcaso et al. (1992). The average values of density of different rock layers ranged from 2960 kg/m^3 for Layer-1 to 2670 kg/m^3, for Layer-8. Young's Modulus of 127.80, 124.30, 120.08, 90.30, 107.60, 65.50, 60.50 and 57.80 for layers 1, 2, 3, 4, 5, 6, 7 and 8, respectively were calculated (using equation [2], Timosenko and Goodier, 1970) in accordance with the homogeneity of rock rheology.

$$\upsilon = \frac{1}{2}\left[1 - \frac{1}{(V_p/V_s)^2 - 1}\right] \quad \cdots\cdots [1]$$

$$E = \rho V_p^2 \frac{(1+\upsilon)(1+2\upsilon)}{(1+\upsilon)} \quad \cdots\cdots [2]$$

Where E= Young's Modulus, Vp = P-wave velocity, ρ = density and υ = Poisson's ratio. In the segment our study, the P-wave velocities of the upper and lower crust were obtained from Introcaso et al. (1992) to calculate (using equation *[1]*) Poisson's ratio of 0.253. The mean P-wave velocities range 7.05 km/s for Layer-1 to 5.2 km/s for Layer-8. A constant V_p/V_s ratio of 1.74 was chosen from Graeber and Asch (1999), where they stated that the average V_p/V_s ratio is low (<1.74) in the upper and lower crust and high (>1.74) in the deep crust of the central Andes. So, the initial S-wave velocities were set using a constant V_p/V_s ratio of 1.74 by them. We calculated values of S-wave for partial requirements. The two other physical parameters such as internal friction angle ϕ, and cohesion C, have been obtained from the Handbook of Physical constant (Sydney et al., 1966) and did slight manipulation in accordance with compositional constituent and tectonic occurrence of individual Layers from 1 to 8.

6. Boundary condition

There is general agreement that the current phase of mountain building in the Andes has occurred over much of al least the late Cenozoic, with significant uplift during much of Miocene period and the Andes can be considered to be evolving in a steady state (Richardson and Coblentz, 1994). According to Coblentz and Richardson (1996), the origin of E-W compressive stress regime in the South American Plate results from the interaction between the ridge push force and the collisional forces acting along the western margin. The South American intraplate stress field likely results the interaction

of two principal tectonic processes: (1) buoyancy or topographic forces (dominated by the ridge push force acting along the Mid-Atlantic Ridge) and (2) compressional stresses transmitted across the plate boundaries (dominated by the forces along the Peru-Chile Trench).

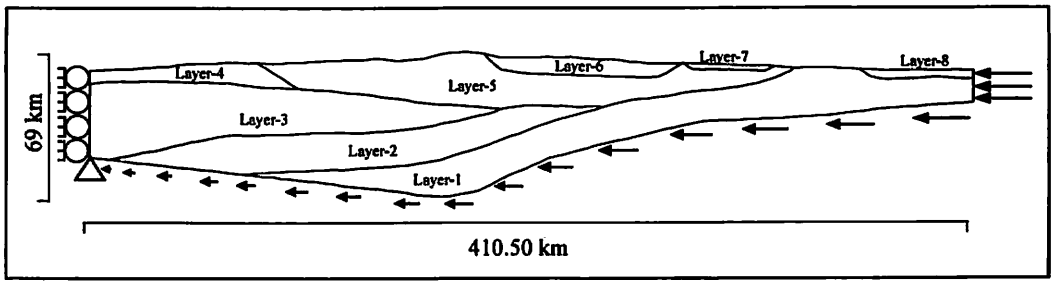

Fig.8 Imposed boundary condition of the model

In our E-W transect along 32°S, force generated due to the convergence of Nazca plate, has been considered as the prime driving forces of the crustal deformation. This assumption is reflected in the boundary conditions used in the present study. The boundary condition applied to the model is shown in Fig.8. The upper surface of the model is free and represents the Earth's surface. Horizontal convergence displacements or velocity (average velocity of 6.50 cm/yr; Klotz et al., 2001) of the Nazca plate have been applied along the bottom side of the crustal layers. Equivalent horizontal nodal displacement has also been applied along the right side of the model. Free-slip boundary conditions have been used along the left wall of the model such that the left side is fixed in the horizontal and free in the vertical dimension. The bottom, representing undeformable Moho, is fixed in the vertical and free in the horizontal dimension. The arrows (Fig. 8) are not drawn to scale. Arrows designated in the bottom are gradually decreases from the right side to the left and finally zero along vertical dimension to the left side.

7. Method of solution

7.1. Finite element technique

The Finite element method has been introduced as a powerful and widely used numerical technique, which deals with the various problems. It is defined as a computer-aided mathematical technique for obtaining approximate numerical solutions to the abstract equations of calculus that predicts the response of physical systems subjected to external influences. This introductory definition of the method identifies the broad spectrum of its applications in areas of engineering, science applied mathematics and recently for the study of structural geological problems.

An important approach for the restoration of geological problem is elastic

deformation of rocks body related to two major physical properties such as Young's modulus and Poisson's ratio (Timoshenko and Goodier, 1970). In our modeling, an approach similar to that of elastic properties of rock has been applied by a computer-aided program coded by Hayashi, unpublished software (2002). Primarily based on a geological cross-section including deep structures (Fig.4) by Cristallini and Ramos (2000) followed after the crustal gravity-seismic model of Introcaso el al, (1992), a two-dimensional finite element model of the area has been constructed (Fig.6).

Here, a summary of how the method generally works is described. The cross-section of the problem is divided into smaller regions or subdomains, called elements. Adjacent elements touch without overlapping, and there are no gaps between the elements. The shape of the elements is intentionally made as simple as possible, such as triangle and quadrilaterals in two-dimensional model. The nodes and elements are collectively referred to as a mesh. The process of defining the size, shapes and locations of the elements, and assigning numbers to each node and element is called mesh generation. We use a procedure of mesh generation based on triangular elements because a planar triangle is the most easy-going geometry for an element in 2-dimensional finite element analysis. The model composed of an assembly of 2699 elements and 1456 nodes with mesh of more or less similar sizes with spatial dimensions of 410.50km length by 69km depth. The elements used are three-node, isoparametric triangles, with linear shape functions and thus constant strain and stress. This simplified model is constructed by using finite element code developed by Hayashi (unpublished) and EPS girding technique (Hayashi, 2002), to determine the stress field and failure elements assuming the linear elastic behavior of materials under plain strain condition. Therefore, the geological section's block that is being transformed in a finite element mesh is adopted with a mesh of constant-strain triangular elements. In this numerical calculation, all deformation directly related to failure of rock layers is generally simulated by elastic behavior of rocks.

7.2. Mohr-Coulomb Failure Criterion

During the last few decades, many numerical modeling have been carried out to examine the failure criterion of rock materials. The most frequently used criterion for brittle failure of rocks is the Mohr-Coulomb criterion. Although many failure criteria have been developed, but, the Mohr-Coulomb failure criterion was chosen because it is commonly used in the study of rock mechanics to determine the peak stress of a material subjected to various confining stresses.

In two-dimensional case, this criterion involves only the maximum and minimum principal stresses, σ_1 and σ_3, and therefore assumes that the intermediate stress σ_2 has no influence on rock strength (Al-Ajmia and Zimmerman, 2006). Following that theme, Hayashi (unpublished) developed a finite element method to construct a two-dimensional geological cross-sectional-based numerical model for prediction of inhomogeneous rock

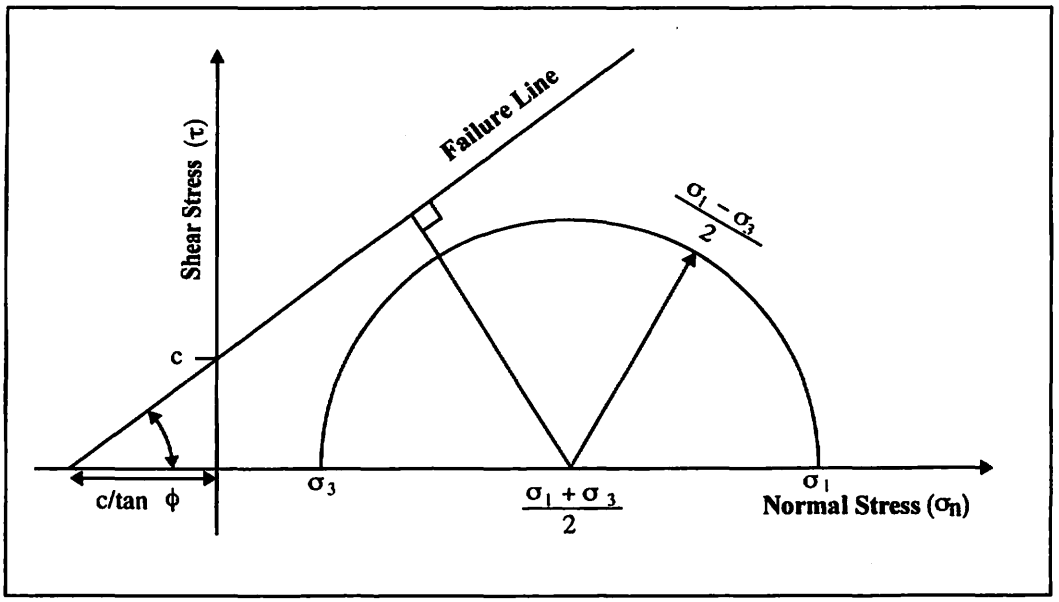

Fig.9 Construction of Mohor-Coulomb failure envelope demonstrating the concept of failure proximity (After Melosh and Williams, 1989), where c, is cohesive strength and f is the angle of internal friction

failure behavior under displacement or velocity loading conditions. In this conventional method, the Mohr-Coulomb and shear stress failure criteria are used to examine the failure behavior of an element at a specific point or discontinuity within a layer. In Mohr-Coulomb, the failure criterion consists of normal, σ_n, and shear stress, τ, axes and a failure envelope (Fig. 9) just touching all possible critical combinations of principle stresses, σ_1 and σ_3. The criterion describes a linear relationship between normal and shear stresses (or maximum and minimum principal stresses) at failure. The direct shear formulation of the criterion is given by equation (1).

$$\tau = c + (\sigma_n) \tan\phi \quad \cdots\cdots (1)$$

where, c is the cohesive strength and ϕ is the angle of internal friction of rock bodies (Melosh and Williams, 1989).

In case of plane strain condition, which is the concentric theme of our model, it is possible to calculate the third principal stress axis, σ^* which is perpendicular to $(\sigma_1-\sigma_2)$ plane and calculated as

$$\sigma^* = \upsilon (\sigma_1+\sigma_2) \quad \cdots\cdots (2)$$

Where υ is the Poisson's ratio (Timosenko and Goodier,1970; Hayshi and Kizaki, 1972). As the calculated values of σ_1, σ_2 and σ^* of every element of model is defined as the maximum, intermediate and minimum principal axes of stress respectively. These values in 2-D stress field condition of every element in model is commensurated with the newly calculated principal stress values σ_1, σ_2 and σ_3 (equivalent to σ^*). According to stress field

and failure vulnerability of rock materials of model, it is possible to predict the location where fault will develop.

Failure begins when the Mohr's circle first touches the failure envelope. This happened under the situation when the radius of the Mohr's circle, $(\sigma_1-\sigma_3)/2$ is equal to the perpendicular distance from the centre of the circle at $(\sigma_1+\sigma_3)/2$ to the failure envelope (Melosh andWilliams,1989).

$$\left(\frac{\sigma_1-\sigma_3}{2}\right)_{faihure}=c\cos\phi+\left(\frac{\sigma_1+\sigma_3}{2}\right)\sin\phi \quad \cdots\cdots(3)$$

The proximity of failure P_f is defined as the ration between the effective stress $\left(\frac{\sigma_1-\sigma_3}{2}\right)$ and the failure stress $\left(\frac{\sigma_1-\sigma_3}{2}\right)_{failure}$ and express by the following equation,

$$P_f=\left[\frac{\left(\frac{\sigma_1-\sigma_3}{2}\right)}{\left(\frac{\sigma_1-\sigma_3}{2}\right)_{failure}}\right] \quad \cdots\cdots(4)$$

If the value of P_f is less than 1.0, the Mohr circle is within the failure envelope and imply no fault developed, but faulting occurred when the P_f value exceeds 1.0.

8. Modeling results

8.1. Stress distribution

In order to subject the deformed fold-and-thrust belts structure to a horizontal compressional stress field, we choose to demonstrate our modeling results by applying horizontal displacement rate (average velocity of 6.50 cm/yr; for Nazca plate) from a minimum of 1000 m up to a maximum of 10000 m. The spatial distribution of stress with its magnitudes shown in the Figures10a, 10b,10c and 10d, where σ_1 is the maximum principal stress, and σ_3 is the minimum principal stress aligned along the horizontal and vertical arms respectively in the two-dimensional section view. In compressional regime, the maximum principal stress (σ_1) is horizontal, whereas the minimum (σ_3) is vertical. Richardson and Coblentz (1994) stated that the vertical shear stress within the lithosphere for Andean-style topography is negligible. Our model under convergence boundary conditions, where the principal stress σ_1 is horizontal throughout most of the layers (Figs.10a, 10b, 10c and 10d), imply that the nature of experimental stress field is compressive, although minute tensional stress occurred within few elements. Stress magnitude sharply increases with respect to gradual increase of displacement rate.

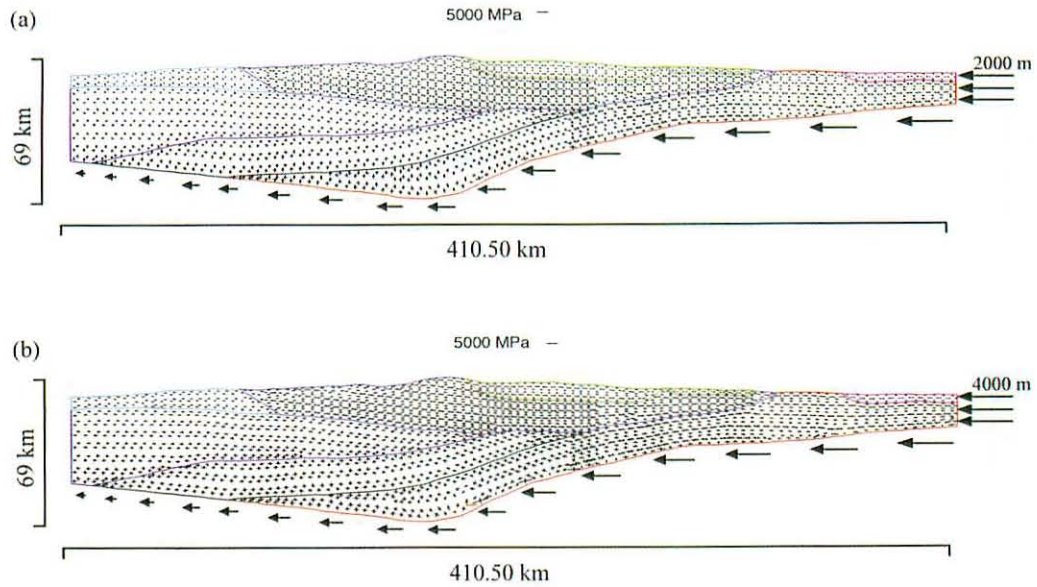

Fig.10a-b Stress distribution, orientation and magnitude of the model for convergent displacement of (a) 2000m and (b) 4000m. Black and red colored straight lines represent compressional and extensional stress, respectively

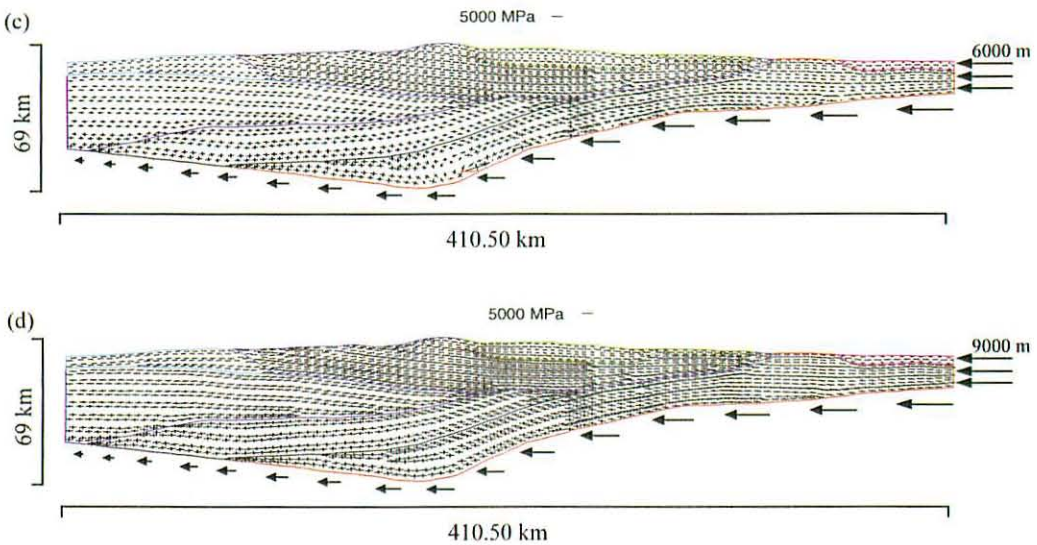

Fig.10c-d Stress distribution, orientation and magnitude of the model for convergent displacement of (a) 6000m and (b) 9000m. Black and red colored straight lines represent compressional and extensional stress, respectively

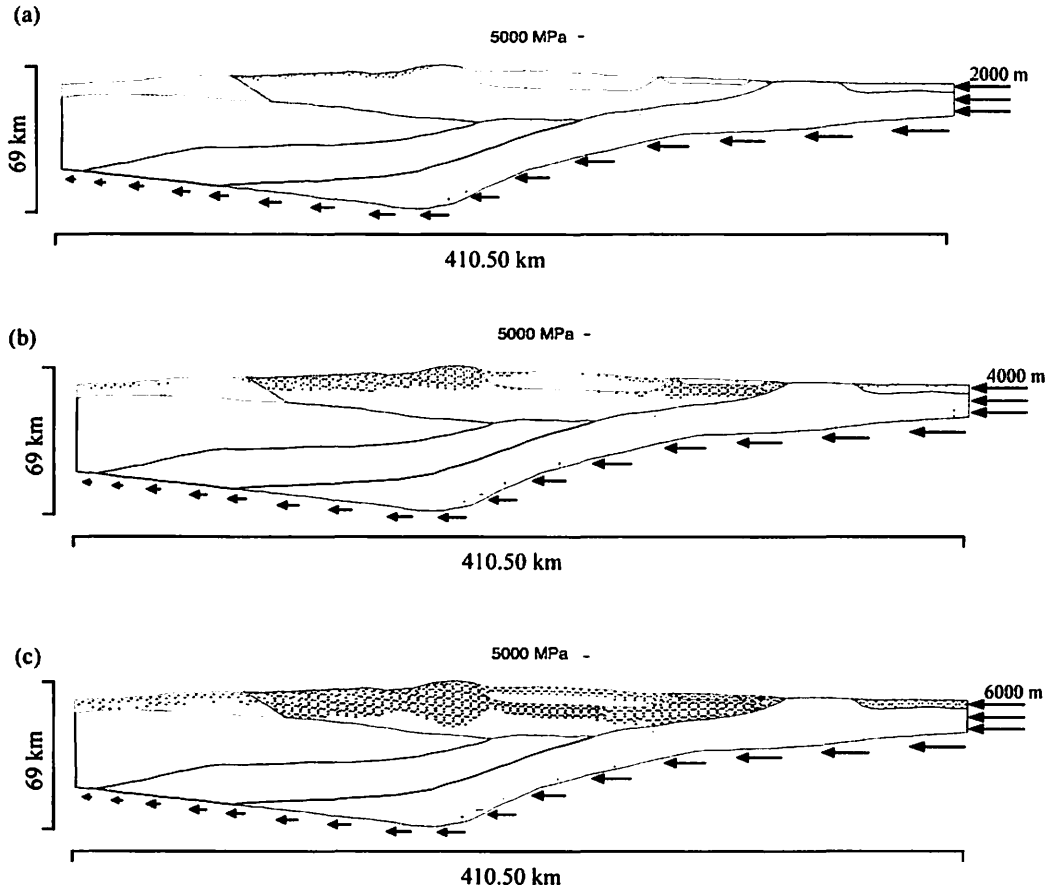

Fig.11a-c Failure of elements of the model under (a) 2000m, (b) 4000m and (c) 6000m convergent displacement rate. Black and red colored straight lines represent compressional and extensional stress, respectively

8.2. Stress distribution within failure of elements

The modeling result is presented based fundamentally on the balanced geological section, the stress regime, overall elastic rheology and plane strain condition. We examined failure of elements in each elastic crustal layer by applying a sequence of displacement rate from 1000 m to 10000 m. For 0 m displacement i. e. in gravitational force, no reasonable amounts of elements were failed in the model layers. In case of 1000 m displacement rate, no compressive failure was obtained inside the Layers of 4, 5, and 6 (Fig. 11a); failure started from 2000 m displacement rate, a very few failures were observed within Layer-5 (Fig. 11b) and gradually increased with imposed displacement rates. In case of 9000 m displacement values, we adopted best fits result where most of the failure of elements concentrated within the Layers of 4, 5, and 6 (Fig.11c) up to depth ranges about 8-20 km-thick lithosphere.

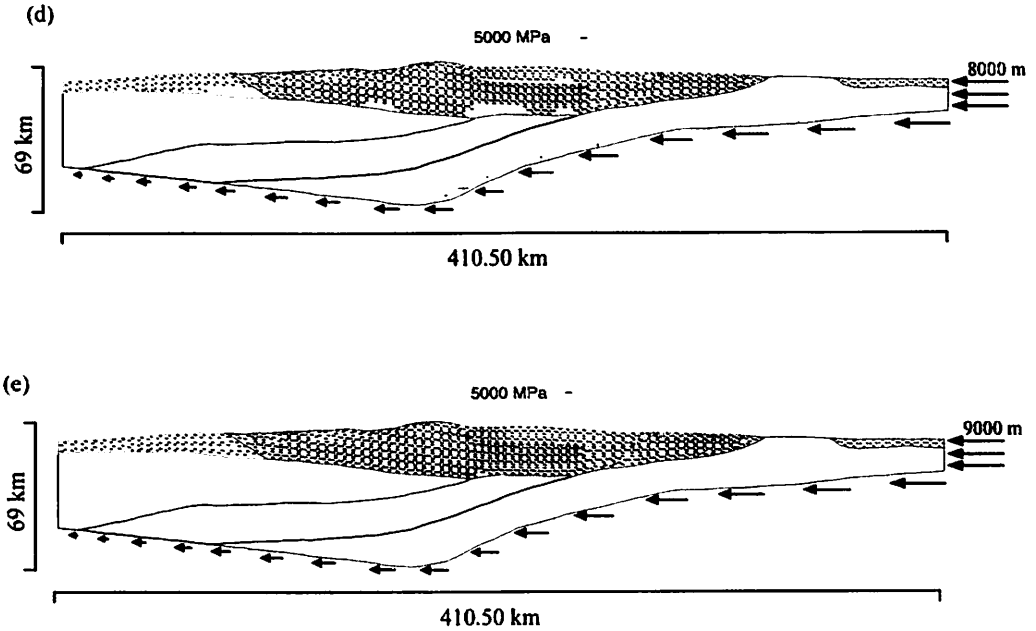

Fig.11d-e Failure of elements of the model under (d) 8000m, (e) 9000m convergent displacement rate. Black and red colored straight lines represent compressional and extensional stress, respectively

9. Focal-Mechanism Solutions of study area

9.1. Predominance of horizontal compression

Jordan et al. (1983) stated that a strong horizontal east-west grouping of compressional axes of the focal-mechanism solutions exists for the upper plate earthquakes within the entire region from Ecuador to Argentina and in the foreland and Eastern Cordillera of Colombia (Fig.12). Although dip-slip solutions predominate, strike-slip orientations are found in parts of Peru, Ecuador, and Colombia where the trend of the Andes is most transverse to the regional stress orientation. The average stress direction (obtained from focal mechanism data) and the inferred direction of relative motion across the Nazca-South American plate boundary are sub-parallel. This coincidence suggests that the over-all convergence of the two plates is an important determinant of the stress within the upper plate in contrast to more localized and variable effects of uplift, magmatic intrusion, or other upper-plate processes. Focal-mechanism solutions of several earthquakes located along the magmatic arc of Chile-Argentina reflect the over-all east-west compressive stress (Fig. 12, e. g. earthquake events 64, 71).

9.2. Relationships of seismicity to Late Cenozoic deformation of the Upper Plate

There is considerable seismic activity within the upper 50 km of the overriding South American plate. This seismic activity is well separated from the inclined seismic zones and

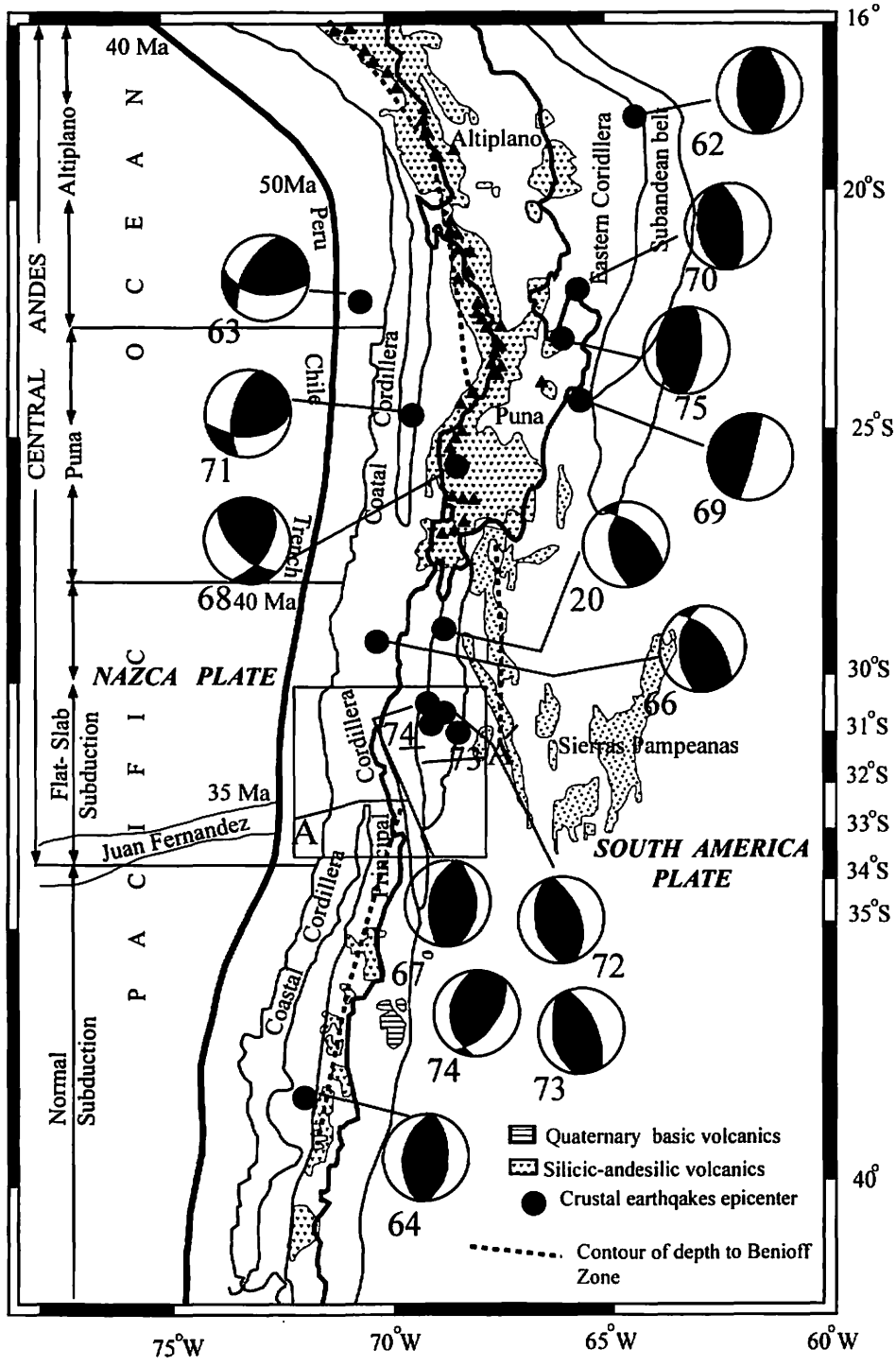

Fig.12 Equal area projections of focal mechanism for well-determined shallow earthquakes for same area as Figure.2. In flat-slab area, between about 28°S and 33°S, most of the events are compressional and occurred between in depth from 10 to 25 km (Jordan et al., 1983)

probably occurs in the crustal part of the South American plate. Deformation at middle and upper-crustal depths is demonstrated by reliable determinations of depths of earthquakes and most of the depths are between 10 and 25 km, but a significant minority occurs at depths of 25 to 30km. Depths of many of the events are clearly below the sedimentary section and indicate compressional deformation of the basement. In flat-slab segment of Chile-Argentina, the areas of significantly seismicity characterized by focal mechanism solutions with horizontal compressive axes, the latest Neogene structures are dominated by reverse faulting and folding, and indicative of important crustal shortening (Jordan et al., 1983).

Five earthquakes exemplify the thick-skinned Pampeanas Ranges deformational style (events 20, 67, 72, 73 and 74) (Fig.12). Event 72 was the large (Ms = 7.3) earthquake of November 23, 1977, followed by the aftershocks 73 and 74. The depths of 15 to 20 km indicate faulting in basement. The dips of nodal planes, all between 30° and 60°, indicate reverse faulting rather than faulting along a nearly horizontal decollement or along nearly vertical faults. These results are in good agreement with the geological evidence for uplift of basement blocks exposed in the Pampeanas Ranges by movement along reverse faults. Many of the nodal planes strike north-northwest, oblique to the northerly strike of the convergent plate boundary (and the strike of the main Cordilleras) but more nearly parallel to a common trend in the basement uplifts of the Pampeanas Ranges. This suggests that the strain pattern of the Pampeanas Ranges is partly controlled by major pre-Andean basement structures. Event 20 also displays the north-northwest trend and, with a depth of 32 km, is quite clearly located in the basement. A large earthquake (Ms = 7.4) in 1944 destroyed the city of San Juan (31°31′ S to 68°30′ W), located near the boundary between the predominantly east-verging Precordillera-Frontal Cordillera system and the mainly west-verging western Pampeanas Ranges (Jordan et al., 1983).

10. Discussions

The South Central High Andean fold-and-thrust belts from 30°S to 33°S in Chile and Argentina is principally due to crustal shortening concentrated at the eastern-most edge of the Andean orogen. In this study, we intend to show the main features of the fold-and-thrust belt with a specific initial geometry related to basement-involved deformation from the elastic rheological justification, rather than to make quantitative statements about to the style of thrusting, changes in fault attitude in distinct parts of the model. We use the two-dimensional finite element technique coded by Hayashi (2002), which solves for force equilibrium and includes brittle as well as elastic rheology, to examine the crustal layers behaviors of our model under compression. In order to investigate the dynamics that led to the deformation of the fold-and-thrust belts in the SCHA area, we have simplified the geometry of the orogenic belt (Fig. 5). A number of simplifications from a geological cross-section (by Introcaso, et al., 1992: Cristallini and Ramos, 2000) were used to make

the model. The crustal lithosphere was divided into eight layers such as Layer-1 to 8 (see Table1) based on density variations and individual rock layers from Paleozoic basement to Quaternary age. The model is extended up to 410.50 km and consists of a 69 km thick continental lithosphere; and composed of an assembly of 2699 elements and 1456 nodes in a state of plane strain.

In order to incorporate the brittle deformation mechanisms of the model, we adopt an elastic rheology as imposed by Richardson and Coblentz (1994) in the Andean region. Generally, in elastic rheology, Young's Modulus, Poisson's ratio, density, friction angle and cohesion play a great role in state of stress concentration and strain rate in a region. Values of Young's Modulus of the layers were calculated in accordance with the homogeneity of rock rheology. A constant Vp/Vs ratio of 1.74 was chosen from Graeber and Asch (1999) to calculate Poisson's ratio of 0.253. The density values were obtained from a 2D Andean crustal gravity-seismic model along 33°S that was carried out by Introcaso et al. (1992). The average values of density of different rock layers ranged from 2670 kg/m^3 to 2960 kg/m^3 according to depth variations from top to bottom. Other two parameters, i.e. friction angle and cohesion were taken from the empirical values of preferred rock materials, calculated after Hand book of Physical constant (Sydney et al., 1966). Later, a series of calculations were performed by slightly manipulating the empirical values of those two parameters. Finally, as more reasonable values for best fits results were chosen as described in Table 2 and Fig. 7.

The model is designed to show the important controlling factor in an environment under compression. Horizontal convergent displacement of Nazca plate has been considered as the prime driving forces for the development of upper plate fold-and-thrust belts in this region. This assumption is reflected in the boundary conditions of E-W transect (Fig.8). We imposed 1000 m, 2000 m, 3000 m, 4000 m and 5000 m, 6000 m, 7000 m, 8000 m, 9000 m and 10000 m displacement or velocity rate successively. The modeling results show that the number of failure of elements increases gradually in accordance with increasing displacement values. The principal stress and failure of elements in the model were influenced by the variation of different physical properties especially high cohesion and friction angle and changes in displacement boundary conditions. The first failure started from 2000 m (Fig.11a) and was concentrated only in upper part of Layer-5, and a minute changes were observed in case of 4000 m (Fig.11b) rate of displacement. Even though, for values of 6000 m (Fig.11c) and 800 m (Fig.11d), we didn't adopt any reasonable results. In case of 9000 m displacement (Fig.11e) values, we adopted best fits result where most of the failure elements concentrate within and along the slip planes of Layers 4, 5, and 6 indicating locations of Precordillera, Frontal, Main and Coastal Cordillera, respectively.

Our elastic modeling results are in good agreement with the study of focal mechanism solutions of Jordan et al. (1983). Focal-mechanism solutions of several earthquakes located along the magmatic arc of Chile-Argentina reflect the over-all east-west compressive

stress. Most of the events (Fig.12) occurred at the depths of 15 to 20 km indicate faulting in basement. Event 66 occurred near the boundary between the Precordillera (Layer-4 in our model) and the Frontal Cordillera (Layer-5), in the area of inferred thin-skinned tectonics, has a thrusting focal mechanism (Jordán et al., 1983).

In this compressional analysis, most of the basement-involved deep thrust (about 20 km), regarding to compressional deformation, occurred on the upper crustal part and lie inside the Layer-4, 5 and 6, respectively (Fig.11e). Formation of several shear bands due to failure of elements between Layers 4, 5 and 6 and Layers 1, 2 and 3 is a reason to change rheology in the zone, leading to deformation-induced competence contrast. The results of Klotz et al. (2001), a study on crustal deformation in the central and southern Andes derived from GSP technology, suggested that all of the plate convergence along the Chilean trench currently accommodated by the build-up of elastic strain which leads to a high probability of future earthquakes in this region. In addition, Ramos et al. (2002) notified a Neo-tectonic study based on GPS measurement, where the deformation in the thrust front of the Precordillera is active. So, both study coincide to our modeling results.

Finally, it can be mentioned that variations in the lithospheric component of stress are related to shear zones cutting through the fold-and-thrust belt. The far-field major principal component of the tectonic stress field was found to be oriented approximately E-W. This is consistent with the most recent direction of regional crustal shortening based on kinematic analysis of faults.

11. Conclusions

We have used an elastic finite element model to evaluate the lithospheric state of stress related to fold-and-thrust belts in the SCHA region. Several important points of our modeling are concluded as follows-

(1) Subducting Nazca plate-induced convergent displacement is responsible for the basement-involved thrusting along core of the South Central High Andes.

(2) Brittle failure mechanism, dominated by compressional deformation at middle and upper-crustal depths between 10 and 25 km, is adopted for the development of basement-involved fold-and-thrust belts in the region.

(3) Most of compressional deformation of elements were concentrated within Layers-4 (Precordillera), Layer-5 (Frontal and Main Cordillera) and Layer-6 (Main Cordillera) rather than other layers (Fig.11e), which imply that fold-and-thrust development in this belt were associated with amendment in rheology that leading to deformation-induced competence contrast.

(4) Finally, it can be mentioned that variations in the lithospheric component of stress are related to shear zones cutting through the fold-and-thrust belt on flat-slab segment along 32°S in the Chile and Argentinean Andean.

Acknowledgement

M. R. I. would like to express special appreciation to Ministry of Education, Culture, Sports, Science and Technology of Japan (Monbukagakusho) for financial support that enable me to complete this research effort.

References

Abascal, L. V., 2005, Combined thin-skinned and thick-skinned deformation in the central Andean foreland of northwestern Argentina, Journal of South American Earth Sciences, vol. 19, pp. 75-81

Al-Ajmia, A. M., and Zimmermana, R. W., 2006, Stability analysis of vertical boreholes using the Mogi-Coulomb failure criterion. International Journal of Rock Mechanics & Mining Sciences (in press)

Alvarez P. P. and Ramos, V. A., 1999, The Mercedario rift system in the principal Cordillera of Argentina and Chile (32°SL). Journal of South American Earth Sciences, 12, 17-31

Cahill, T., and Isacks, B., 1992, Seismicity and shape of the subducted Nazca Plate. Journal of Geophysical Research, 97, 17503-17529.

Coblentz, D. D., and Richardson, R. M., 1996, Analysis of the South American intraplate stress field. J. Geophys. Res., 101, No B4, 8643-8657.

Costa, E., and Vendeville, B.C., 2002, Experimental insight on the geometry and Kinematics of fold-and-thrust belts above weak, viscous evaporitic Décollement. Journal of Structural Geology, 24, 1729-1739.

Cristallini, E. O. and Ramos, V. A., 2000, Thick-skinned and thin-skinned thrusting in the La Ramada fold and thrust belt: crustal evolution of the High Andes of San Juan, Argentina (32°SL). Tectonophysics, 317, 205-235

Davis, D. M., Suppe, J., and Dahlen, F.A., 1983, Mechanism of fold-and-thrust belts and accrectionary wedges. Journal of Geophysical Research, 88,1153-1172.

Davis, D. M., and Engelder, T., 1985, The role of salt in fold-and-thrust belts. Tectonophysics, 119, 67-88.

Doglioni, C., and Prosser, G., 1997, Fold uplift versus regional subsidence and sedimentation rate. Marine and Petroleum Geology, 14, 179-190.

Epard, J. L., and Escher, A., 1996, Transition from basement to cover: a geometric model. Journal of Structural Geology, 18, 533-548.

Gutscher, M. A., Malavieille, J., Lallemand ,S., and Collot, J. Y., 1999, Tectonic segmentation of the North Andean margin: impact of the Carnegie Ridge collision. Earth and Planetary Science Letters, 168 , 255-270.

Graeber, F. M., and Asch, G., 1999, Three-dimensional models of P wave velocity and P-to-

S velocity ratio in the south central Andes by simultaneous inversion of local earthquake data. J. Geophys. Res., 104, No. B9, 20237-20256.

Hayashi, D., 2002. Unpublished FEM software.

Hayashi, D., Kizaki, K., 1972, Numerical analysis on migmatite dome with special reference to finite element method. Jour. Geol. Jap., 78, 677-686.

Introcaso, A., Pacino, M. C., and Fraga, H., 1992, Gravity, isostasy and Andean crustal shortening between latitudes 30 and 35°S. Tectonophysics, 205, 31-48

Jordan, T. E. and Allmendinger, R.W., Damanti J., and Drake., R.,1993. Chronology of motion in a complete thrust belt: the Precordillera, 30°-31°S, Andes Mountains. J. Geol., 101, 133-156.

Jordan T. E., Isacks, B. L., Allmedinger, R. W., Brewer, J. A., Ramos, V. A., Ando, C. J., 1983, Andean tectonic related to geometry of subducted Nazca plate. Geol. Stud. of American Bull., 94, 341-361.

Kley, J., Monaldi, C.R., and Salfity, J., 1999, Along-strike segmentation of the Andean foreland: causes and consequences. Tectonophysics, 301, 75-94.

Klotz, J., Khazaradze, G., Angermann, D., Reigber, C., Perdomo, R., Cifuentes, O., 2001, Earthquake cycle dominates contemporary crustal deformation in the Central and Southern Andes. Earth and Planetary Science Letters, 193, 437-446.

Koyi, H. A., and Cotton, J., 2004, Experimental insights on the geometry and kinematics of fold-and-thrust belts above weak, viscous evaporitic decollement; a discussion. Journal of Structural Geology, 26, 2139-2143.

McQuarrie, N., 2004, Crustal scale geometry of the Zagros fold-thrust belt, Iran. Journal of Structural Geology, 26, 519-535

McQuarrie, N., 2002, Building a high plateau: the kinematic history of the central Andean fold-thrust belt, Bolivia. Geol. Soc. Amer. Bull., 114, 950-963.

Melosh, H. J., Williams, C.A., 1989, Mechanics of graben formation in crustal rocks: A Finite Element analysis. J. Geophys. Res., 94, 13961-13973.

Morata, D., and Aguirre, L., 2003, Extensional Lower Cretaceous volcanism in the Coastal Range (29°20'-30°S), Chile: geochemistry and petrogenesis. Journal of South American Earth Sciences, 16, 459-476.

Pérez, D. J., 2001, Tectonic and unroofing history of Neogene Manantiales foreland basin deposits, Cordillera Frontal (32°30'S), San Juan Province, Argentina. Journal of South American Earth Sciences, 14, 693-705.

Ramos, V. A., Cristallini, E. O., Perez, D., 2002, The Pampean flat-slab of the Andes. Journal of South American Earth Science, 15, 59-78.

Ramos, V. A., Cegarra, M., and Cristallini, E. O., 1996, Cenozoic tectonics of the High Andes of west-Central Argentina (30-36°S latitude). Tectonophysics, 259, 185-200.

Richardson, R. M., and Coblentz, D. D., 1994, Stress modeling in the Andes: Constraints on the South American intraplate stress magnitudes. J. Geophys. Res, 99, No B11,

22015-22025.

Sydney, P., Clark, J.R.,1966, Handbook of Physical constants. Geol. Soc. Am. Mem.,

Tassara, A., 2005, Interaction between the Nazca and South American plates and formation of the Altiplano-Puna plateau: Review of a flexural analysis along the Andean margin (15°-34°S). Tectonophysics, 399, 39-57

Talukder, M. W., and Hahashi, D., 2006, Numerical simulation f faults in Southern Bolivia and Northern Argentinean Orocline, Central Andes. Bull. Faculty of Science, University of the Ryukyus, 81, 41-70.

Taylor, G.K., Grocott, J., Pope, A., and Randall, D.E., 1998, Mesozoic fault systems, deformation and fault block rotation in the Andean forearc: a crustal scale strike-slip duplex in the Coastal Cordillera of northern Chile. Tectonophysics, 299, 93-109.

Timoshenko, S. P., Goodier, J. N., 1970, Theory of Elasticity. McGraw Hill Book Company. London, Third edition, p 567, international edition, p 488.

Wdowinski, S., and Bock, Y., 1994, The evolution of deformation and topography of high elevated plateaus, 2, Application to the central Andes. J. Geophys. Res., 99, 7121-7130.

Yuan, X., Sobolev, S. V., and Kind R., 2002, Moho topography in the central Andes and its geodynamic implications. Earth and Planetary Science Letters, 199, 389-402.